Quantum Electronics **52** (3) 254–261 (2022) ©2022 Kvantovaya Elektronika and IOP Publishing Limited

https://doi.org/10.1070/QEL18006

Mid-IR optical parametric oscillation and second harmonic generation of repetitively pulsed output of a fibre-laser pumped Tm^{3+} : YAP laser in a fan-out periodically poled MgO : $LiNbO_3$ crystal

O.L. Antipov, D.B. Kolker, A.A. Dobrynin, Yu.A. Getmanovskii, V.V. Sharkov, M.A. Chuvakova, A.R. Akhmatkhanov, V.Ya. Shur, I.A. Shestakova, S.V. Larin

Abstract. **The nonlinear optical frequency conversions of repetitively pulsed output of a 1941-nm Tm^{3+} : YAP laser pumped by a cw 1670-nm fibre laser are studied experimentally. Both mid-IR optical parametric oscillation (OPO) and second harmonic generation (SHG) are obtained in the same periodically poled MgO : $LiNbO_3$ crystal with a fan-out domain design by tuning the grating period and temperature. The energy conversion efficiency of the degenerate OPO at 3820–3970 nm exceeds 43% at a 0.5 kHz repetition rate, while the energy conversion efficiency of SHG at 970.5 nm reaches 34%.**

Keywords: *solid-state lasers, two-micrometre wavelength region, fibre lasers, nonlinear optical frequency conversion, periodically poled MgO : $LiNbO_3$ crystals, optical parametric oscillator, mid-IR range, frequency doubling.*

1. Introduction

Nonlinear optical frequency conversions make it possible to significantly broaden the wavelength range of high-power coherent laser radiation. Two-micrometre range lasers at wavelengths of 1900–2100 nm, widely used in various fields (surgery and urology, precision material processing, remote environmental diagnostics, etc.), are good sources of pump radiation for optical parametric oscillators (OPOs) in the mid-IR range with signal and idler waves at $\lambda = 3.5–5$ μm [1, 2]. Using frequency doubling and harmonic generation, the radiation of these lasers can also be converted into the short-wavelength near-IR or visible wavelength range [3, 4].

Among solid-state lasers in the two-micrometre spectral range based on crystals doped with Ho^{3+} or Tm^{3+} ions, the highest average output powers for a high beam quality are achieved using coherent pumping by radiation from fibre or solid-state lasers [2, 5–7]. Resonant in-band pumping, which ensures a small quantum defect, makes it possible to obtain with high efficiency an average output power above 200 W in a high-quality beam (with a divergence close to the diffraction limit) in lasers based on Ho^{3+} : YAG crystals (see, for example, Ref. [8]).

When using two-micrometre radiation from lasers based on Ho^{3+} : YAG crystals for pumping OPOs and parametric amplifiers based on nonlinear $ZnGeP_2$ (ZGP) crystals, a power of 160 W and a pulse energy of more than 200 mJ have been recently achieved in the mid-IR range (at wavelengths of 3700–4800 nm) [9, 10]. This turned out to be possible due to the combination of several basic parameters inherent in a nonlinear ZGP crystal: high quadratic nonlinearity and birefringence, as well as thermal conductivity and hardness [11]. A perfect (ideal) ZGP crystal is transparent in the 0.74–8 μm wavelength range, but absorption due to impurities and crystal lattice defects limits its use in nonlinear optics at wavelengths shorter than 2 μm. Limitations on the use of ZGP for high-power laser systems are also associated with the optical breakdown of its surface, whose threshold does not exceed 2–4 J cm^{-2} even for the best samples and can become appreciably lower within a few seconds under repetitively pulsed pumping [11–13].

Oxide nonlinear optical crystals (such as KTP, KTA, $LiNbO_3$, $LiTaO_3$, etc.) that are transparent in the visible and near-IR ranges have a high optical breakdown threshold and are actively used for nonlinear optical conversion in these ranges [2, 14–17]. In periodically poled crystals, the fulfilment of the phase-match conditions for the nonlinear optical interaction is achieved by choosing the period of the structure of ferroelectric domains with the opposite direction of spontaneous polarisation. Due to the difference in sign of the nonlinearity coefficient of these domains, quasi-phase matching is realised. Among all periodically poled oxide structures, periodically poled $LiNbO_3$ doped with MgO (PPMg : LN) has the highest coefficient of quadratic optical nonlinearity and a sufficiently high optical breakdown threshold in the transpar-

O.L. Antipov Institute of Applied Physics, Russian Academy of Sciences, ul. Ulyanova 46, 603950 Nizhny Novgorod, Russia; Lobachevsky State University of Nizhny Novgorod, prosp. Gagarina 23, 603022 Nizhny Novgorod, Russia; Novosibirsk State University, ul. Pirogova 1, 630090 Novosibirsk, Russia; e-mail: antipov@ipfran.ru;
D.B. Kolker Novosibirsk State University, ul. Pirogova 1, 630090 Novosibirsk, Russia;
A.A. Dobrynin, V.V. Sharkov Lobachevsky State University of Nizhny Novgorod, prosp. Gagarina 23, 603022 Nizhny Novgorod, Russia;
Yu.A. Getmanovskii Institute of Applied Physics, Russian Academy of Sciences, ul. Ulyanova 46, 603950 Nizhny Novgorod, Russia; R.E. Alekseev Nizhny Novgorod State Technical University, ul. Minina 24, 603950 Nizhny Novgorod, Russia;
M.A. Chuvakova, A.R. Akhmatkhanov, V.Ya. Shur Ural Federal University, ul. Mira 19, 620002 Ekaterinburg, Russia;
I.A. Shestakova OJSC M.F. Stel'makh Polyus Research Institute, ul. Vvedenskogo 3, stroenie 1, 117342 Moscow, Russia;
S.V. Larin IRE-Polus Research and Technology Association, pl. Vvedenskogo 3, stroenie 5, 141195 Fryazino, Moscow region, Russia

Received 5 January 2022
Kvantovaya Elektronika **52** (3) 254–261 (2022)
Translated by E.N. Ragozin

ency range; furthermore, the production technology of this crystal is the most developed [14–16]. PPMg:LN crystals are used for frequency doubling and for parametric conversion to the mid-IR range up to a wavelength of ~4 μm, above which the multiphonon absorption in them appreciably increases [15]. Another advantage of PPMg:LN crystals is that they can be pumped by radiation from well-developed solid-state lasers at a wavelength of ~1 μm. The power of an OPO in the mid-IR range based on PPMg:LN structures, when pumped at a wavelength of ~1 μm, gradually increases as the quality of the nonlinear crystal improves [18–23]: when the crystal was pumped by ytterbium fibre laser radiation according to the 'master oscillator–amplifier' scheme, an idler-wave output of ~5.5 W at $\lambda = 3.82$ μm was obtained in 2012 [22], and an idler-wave output of 10.8 W at $\lambda = 3.75$ μm was reported in 2022, which was obtained under pumping by the radiation from a repetitively pulsed Yb fibre laser [23]. A certain disadvantage of pumping an OPO at $\lambda = 1$ μm is that only the idler wave falls into the mid-IR range (longer than 3 μm), while the signal wave remains in the near-IR range at λ =1.5–2 μm. Reported in 2020 was an efficient stepwise conversion of fibre laser radiation in PPMg:LN crystals: first, the difference frequency of radiation from ytterbium and erbium lasers was generated (at 1.06 and 1.55 μm, respectively), and then the signal was parametrically amplified at a wavelength of ~3 μm when pumped at λ =1.55 μm [24].

Pumping a PPMg:LN crystal OPO by radiation from two-micrometre lasers makes it possible to generate signal and idler waves in the range of 3.5–4.5 μm. However, nonlinear optical conversion of two-micrometre laser radiation in PPMg:LN has been little studied to date. In PPMg:LN crystals, second harmonic generation (SHG) and higher harmonic generation of thulium fibre lasers at a wavelength of ~1.9 μm were previously implemented [25–27]. Several attempts were made to obtain high-power parametric lasing in the 3.5–4.5 μm region by pumping PPMg:LN structures by pulsed solid-state lasers in the two-micrometre region: Tm:YAG laser at $\lambda = 2012.4$ nm [28], Tm,Ho:YLF laser at $\lambda = 2051$ nm [29], as well as Tm,Ho:$GdVO_4$ laser at $\lambda = 2048$ nm [30]. However, an appreciable absorption in $LiNbO_3$ crystals at a wavelength longer than 4 μm, which significantly affects the long-wavelength idler wave, limited the pulsed energy and the average power of mid-IR OPOs as a whole [28–30]. Reported in our previous works was the parametric conversion in PPMg:LN crystals of Tm^{3+}:Lu_2O_3 ceramics laser radiation (λ ~1.97 μm) with a high pulse repetition rate, but the competition between the parametric conversion and harmonic generation made it difficult to implement both effects with the source used pumping [4, 31].

This paper presents the results of studies of mid-IR OPO and SHG in a PPMg:LN crystal with a fan-out domain structure pumped by a solid-state Tm^{3+}:YAP laser at 1941 nm. The realisation of these two nonlinear optical effects in one crystal turned out to be possible due to the selection of the structure period and temperature. The use of pumping at this wavelength made it possible to obtain efficient optical parametric oscillations of signal and idler waves in a close-to-degenerate regime in the wavelength range of 3.82–3.97 μm, in which the multiphonon absorption of $LiNbO_3$ crystals is still low. In addition, as a result of frequency doubling, radiation was obtained at a wavelength of 970.5 nm.

2. Solid-state Tm^{3+}:YAP crystal laser pumped by fibre laser radiation

Diode-pumped Tm^{3+}:YAP solid-state lasers have gained wide acceptance in recent years due to the possibility of obtaining high power in the cw regime and realising a repetitively pulsed regime with *Q*-switching of the cavity using saturable absorbers or a mechanical device for deflecting the mirror [32–34]. In the present work, the Tm^{3+}:YAP crystal was pumped by fibre laser radiation at a wavelength of 1670 nm corresponding to the $^3H_6 \rightarrow {}^3F_4$ transition line (Fig. 1a). Such resonant pumping of crystals and ceramics doped with Tm^{3+} ions occurs due to an absorptive transition between the same Stark-split levels $^3H_6$ and $^3F_4$, between which the radiative transition of laser amplification occurs (Fig. 1a). This makes it possible to improve the lasing efficiency achievable in the wavelength range 1.9–2.08 μm, and to reduce thermally induced distortions in the active medium compared to the case of cross-relaxation diode pumping [35–37].

For pumping, we used a cw fibre laser at 1670 nm, made on the basis of an erbium laser with an efficient Raman conversion of the wavelength from 1567 to 1670 nm in an ELM-

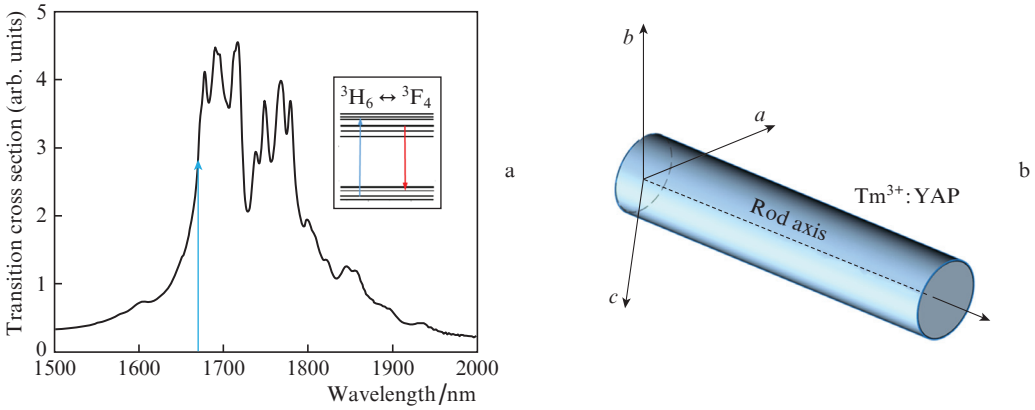

Figure 1. (Colour online) (a) Absorption spectrum of the Tm^{3+}:YAP crystal at the $^3H_6 \rightarrow {}^3F_4$ transition line for radiation polarised along the *c* axis, pumping at 1670 nm is shown by the blue arrow (the inset shows the scheme of pumping and lasing at the $^3H_6 \leftrightarrow {}^3F_4$ transition) and (b) scheme of active-element orientation with respect to crystallographic axes *a*, *b*, *c* of the Tm^{3+}:YAP crystal with lattice periods $a = 5.329$ Å, $b = 7.370$ Å, and $c = 5.179$ Å [39].

1670-50 fibre laser (IRE–Polyus Research and Technology Association, Fryazino, Moscow region, Russia) [38].

The active element (OJSC Polyus Research Institute, Moscow) was cut from a Tm^{3+}:YAP crystal (the density of Tm^{3+} ions is 1 at.%) in the form of a 25-mm long rod 3 mm in diameter, whose axis coincided with the bisector of the angle between the crystallographic axes *a* and *c* of this crystal (Fig. 1b).

Previously, in our preliminary experiments with Tm^{3+}:YAP lasers pumped at 1670 nm, we discovered the possibility of lasing in the cw or repetitively pulsed regime at wavelengths of 1890, 1897, 1938, 1941, 1985, and 1992 nm [40]. Similar multiwavelength lasing with switching from one wavelength to another was earlier studied in $Tm^{3+}:Lu_2O_3$ ceramics pumped at 1670 nm [36, 41]. Therefore, to select and stabilise lasing at a wavelength of 1941 nm, use was made of an L-shaped Tm^{3+}:YAP laser cavity (Fig. 2). The dichroic dielectric mirrors (input and highly reflecting) of this cavity differed greatly in their reflection coefficients at $\lambda = 1941$ nm and in the range of 1980–2000 nm: the highly reflecting mirror at 1941 and 1670 nm had $R > 99.5\%$ and 99%, respectively; the reflectivity of the input mirror at an angle of 45° for s-polarisation exceeded 99% at 1941 nm, and the transmission T of unpolarised pump radiation at 1670 nm was higher than 98%. The output mirror had a low reflectivity R at 1800–1900 nm and 1980–2000 nm, and R was ~50% at the laser wavelength. The input and highly reflecting mirrors were plane, while the output mirror was concave with a radius of curvature of 100 mm. The highly reflecting mirror was located at a distance of 1–2 mm from the end face of the active element. The length of the cavity was varied in the range of 110–130 mm; therefore, taking into account the curvature of the mirrors, the 'cold' cavity was close to hemispherical. Additional selection of the laser wavelength was carried out by an interference filter IF, which was a plane-parallel quartz plate with a thickness of ~90 μm.

Inside the resonator, there was an acousto-optic shutter AOS (OJSC Polyus Research Institute, Moscow) with a 45-mm long quartz optical element. The AOS driver (individual entrepreneur Glazkov A.V., Nizhny Novgorod) generated a high-frequency control signal at a frequency of 50 MHz with a power of up to 20 W. The RF-signal modulation frequency, which determined the repetition rate of laser pulses, was varied from 0.5 to 20 kHz. The distance of the end face of the AOS from the output mirror was varied between 3 and 15 mm.

The diameter of the pump beam, which was ~490 μm (at the level e^{-2} of the peak intensity) at the left (closest to the highly reflecting mirror) end of the active element, was chosen from the condition of its proximity to the calculated diameter of the fundamental mode of the laser cavity, taking into account the thermal lens induced in the active element for an absorbed pump power of 15 W. The simulation was carried out with the Rezonator software package [42], using the following parameters of the crystal, pump, and laser cavity:

Absorbed pump power/W	15
Thermal conductivity coefficient/W cm^{-1} K^{-1})	0.11 [34]
Refractive index	1.92
Thermooptic coefficient $\partial n/\partial T$ K^{-1}	9.7×10^{-6} [43]
Cavity length/mm	120
Focal length of the thermal lens/mm	25
Laser beam radius at the left end of the active element/μm	240

Tm^{3+}:YAP laser generated cw or repetitively pulsed radiation with a time-averaged power of up to 11 or 8 W, respectively (at a pulse repetition rate of 20 kHz) and a high beam quality (Fig. 3). Depending on the output power, the beam quality parameter M^2 determined by the knife-edge method [44] was smaller than 1.1–1.4 (see the inset in Fig. 3). The power was measured with a Coherent PM10 instrument with a FieldMax$_{II}$ indicator or a Gentec UP25N-40S with a SOLO indicator; the spatial structure of the radiation beam was recorded with a pyrocamera Pyrocam IV (Ophir-Spiricon). With an increase in the pump power above 30–32 W and its further increase, the quality of the laser

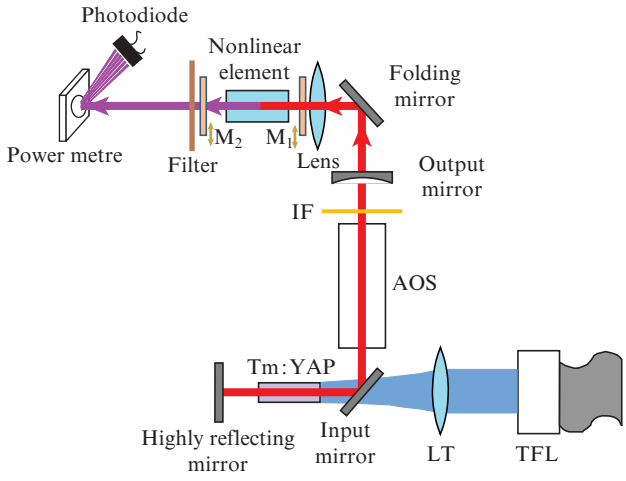

Figure 2. (Colour online) Scheme of an experimental Tm^{3+}:YAP: Tm:YAP crystal laser pumped by a fibre laser and a nonlinear converter based on PPMg:LN (OPO or frequency doubling element): (Tm:YAP) active element of the laser; (TFL) collimating telescope of the fibre laser; (LT) lens telescope for focusing fibre laser radiation; (AOS) acousto-optic shutter; (IF) interference filter; (M_1 and M_2) OPO mirrors.

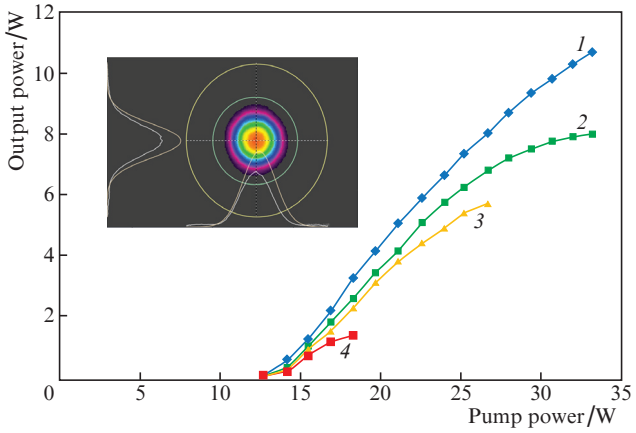

Figure 3. (Colour online) Output power of the Tm^{3+}:YAP laser as a function of the pump power in the cw regime (*1*), as well as in the repetitively pulsed regime for a pulse repetition rate of (*2*) 20, (*3*) 3, and (*4*) 0.5 kHz. The inset shows an image of the laser beam recorded by a Pyrocam IV camera.

beam deteriorated: the appearance of higher transverse modes was observed.

In the repetitively pulsed regime, the highest laser pulse energy and average power, as well as the shortest pulse duration, were limited by the optical damage of the surfaces of the active element and the cavity dielectric mirrors. The highest working energy of laser pulses was 2.7, 2.4, or 1.9 mJ at a pulse repetition rate of 0.5, 1, or 3 kHz, respectively. As the pulse repetition rate decreased, the average power also decreased to ~1.35 W at a frequency of 0.5 kHz. The shortest pulse duration was 35–50 ns at pulse repetition rates of 0.5–3 kHz (Fig. 4a). It should be noted that the above limitations of the radiation parameters of the Tm^{3+}:YAP laser were determined mainly by the intensity of the pulses at the surface of the indicated optical elements. Optical damage occurred in attempts to shorten the laser pulses for a fixed pump power by adjusting the cavity or increasing the RF power in the AOS.

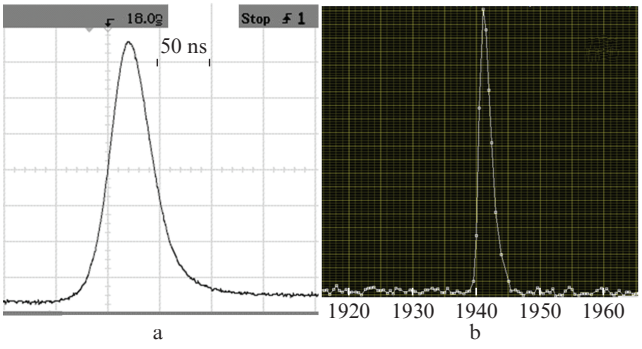

Figure 4. (a) Oscillogram of the laser pulse at a repetition rate of 2 kHz and an average power of ~4.2 W, as well as (b) the laser oscillation spectrum (in nm).

The oscillation spectrum was recorded using an M150 monochromator (Solar Laser Systems, Belarus) and a photodetector made at the Institute of Applied Physics RAS (IAP) based on an InGaAs PIN G8422-03 photodiode (Hamamatsu) with a processing program written at the IAP RAS. Both in cw and repetitively pulsed regimes, the spectrum contained one line at ~1941 nm with a FWHM less than 1 nm (the accuracy of determining the linewidth was limited by the capabilities of the measuring system).

The laser beam had vertical linear polarisation (with a contrast ratio greater than 100:1) determined by the polarisation-selective input mirror and the anisotropic Tm^{3+}:YAP active element.

3. Parametric oscillator based on a PPMg:LN crystal

The radiation of a Tm^{3+}:YAP crystal laser was focused by a lens into a PPMg:LN nonlinear optical element (see Fig. 2). The focal length of the lens varied from 100 to 150 mm and, in view of the geometric divergence of the laser beam, the effective focal length varied from 140 to 210 mm. In this case, the at-focus diameter of the pump beam varied from 250 to 380 μm (in terms of the e^{-2} level of the peak intensity), and the calculated Rayleigh length of the focal waist varied from 23 to 52 mm. The beam diameter in the nonlinear element was determined by the position of the focusing lens and was chosen to maximise the OPO output power and obviate the optical damage at the maximum pump power for an exposure time of up to 30 s.

The PPMg:LN element measuring $50 \times 20 \times 3$ mm ($X \times Y \times Z$) had a fan-out domain structure with a period varying along the crystallographic Y axis from 27.42 to 32.5 μm with a gradient of ~254 nm mm^{-1} (Fig. 5). The period of the fan-out structure was varied by shifting the element along the Y axis [45]. The nonlinear element used in our experiments was fabricated at LLC Labfer (Ekaterinburg) from a $LiNbO_3$ single crystal of a congruent composition doped with MgO (5 mol%) [46]. Antireflection coatings were deposited on the working YZ planes of the crystal surfaces at wavelengths of ~1940 ± 50 nm and ~3.8 ± 0.1 μm (with a residual reflectivity $R < 0.5\%$). The crystal, wrapped in indium foil, was fixed in a radiator and placed in a furnace, whose temperature was controlled by an electronic thermal controller and varied from 280 to 423 K (according to the temperature sensor on the heater) with an accuracy of 0.1 K.

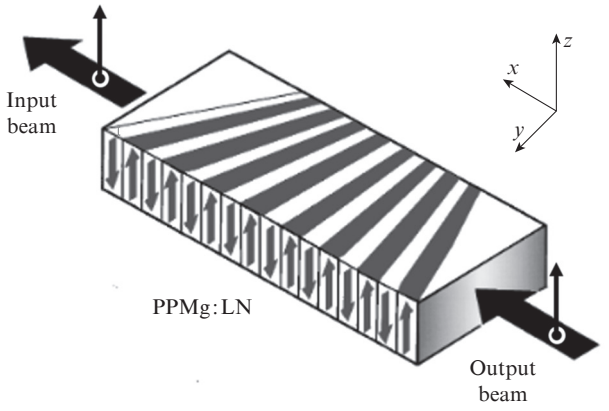

Figure 5. Scheme of excitation of a nonlinear optical element PPMg:LN with a regular fan structure of domains with the opposite direction of spontaneous polarisation (thick vertical arrows). Also shown are the linearly polarised input and output beams and the coordinate system used for the description.

The furnace with a nonlinear optical element was mounted on translation stages and placed in the cavity formed by mirrors M_1 and M_2 (see Fig. 2). The input mirror M_1 was plane and had a high transmittance at a wavelength of 1941 nm ($T > 98\%$) and a high reflectivity in the wavelength range of 3.6–4.1 μm ($R > 99.5\%$). The output mirror M_2 was concave with a radius of curvature of 200 mm, with reflection coefficients $R = 55\%–58\%$ for radiation in the wavelength range of 3.6–4.1 μm and $R > 91\%$ at a wavelength of 1941 nm. The cavity mirrors were located at a distance of 2–3 mm from the ends of the PPMg:LN crystal, and the total length of the OPO cavity was 54–56 mm.

Placed between the OPO and the recording system was a plane mirror filter (dielectric coating on a ZnSe substrate), which was highly reflective for the residual pump radiation at 1941 nm ($R > 99\%$) and had a high transmittance for the radiation in the wavelength range 3.6–4.1 μm ($T = 94\%–95\%$). The recording system included a Coherent PM10 power meter with a $FieldMax_{II}$ indicator and photodetectors manufactured by the IAP RAS based on an FD48-03NS photodiode (AIBI LLC, St.Petersburg) for recording the 3.8–4.1 μm radiation or an InGaAs PIN G8422-03 (Hamamatsu) photodiode for recording the residual radiation at 1941 nm.

The oscillation spectrum was recorded using an M150 monochromator (Solar Laser Systems, Belarus) and a photodetector at a wavelength of 3.8–4.1 μm. The structure of the laser beam after the filter was recorded using a Pyrocam IV camera.

Since the optimal position of the PPMg:LN fan-out structure was initially unknown, the position of the element was varied inside the OPO cavity by shifting along the Y coordinate at ~0.5 mm increments, and the temperature dependence of the output power was measured in each position at ~5 K temperature increments. We chose the position of the element and the temperature at which the radiation transmitted through the monochromator had the strongest component at a wavelength of ~3880 nm. After preliminary determination of the optimal generation conditions, the position of the element was adjusted with an accuracy of ~10 μm and the temperature with an accuracy of 0.1 K. Therefore, the OPO was tuned to the regime of strongest output power, close to degenerate in wavelength (at $\lambda = 3882$ nm).

To find the optimal pump beam diameter (at $\lambda_p = 1941$ nm) in a nonlinear element, we calculated the OPO cavity mode (taking into account the induced thermal lens) employing the Rezonator software package with the parameters of the pump beam, the PPMg:LN crystal, and the cavity, which were used to calculate the induced thermal lens and the radius of the output OPO beam (see below).

According to calculations, good matching of the OPO cavity mode and the pump beam took place at its radius of ~190 μm.

Logarithm of absorption over two passes through non-linear element $2\alpha L$	0.4
Thermal conductivity coefficient/W m^{-1} K^{-1}	4.4 [47]
Refractive index	2.12
Thermooptic coefficient $\partial n/\partial T$/K^{-1}	3.8×10^{-5} [48]
Cavity length/mm	55
Focal length of the induced thermal lens at a pump power of 2 W/mm (for pumping beam radius–μm)*	22.4(150) 36 (190)
Radius of the laser beam and inside the nonlinear element/μm	178–180 190–192

*A focal length of 22.4 mm corresponds to the beam radius 178–180 μm and 36 mm to the radius 190–192 μm.

When focused by a lens with an effective focal length of ~140 mm, the generation of mid-IR radiation was recorded in the temperature range 410–420 K in the longitudinal region of the PPMg:LN nonlinear element with a domain structure period of 30.0–30.1 μm. The found position and temperature of the nonlinear element corresponded to a period of 30.04–30.05 μm optimal for degenerate parametric oscillation, which was calculated using the SNLO program for the indicated temperatures [49].

The output OPO power in the mid-IR range was highest at a temperature of 414–415 K and amounted to 950 mW, and the pulse energy was ~0.95 mJ (total for the signal and idler waves) at an average pump power of 2.4 W (pulse repetition rate: 1 kHz) . The maximum output pulse energy (total for the signal and idler waves) was ~1.18 mJ at a pump pulse energy of 2.7 mJ and a pulse repetition rate of 0.5 kHz; the highest energy conversion efficiency was ~43.5% (Fig. 6).

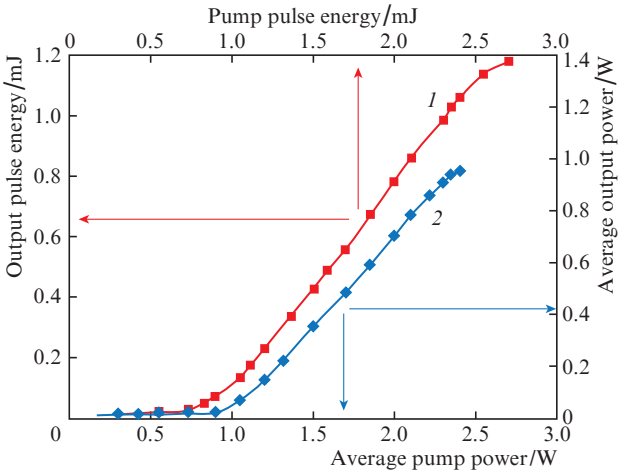

Figure 6. (Colour online) Dependences of the OPO pulse energy (total over the signal and idler waves) on the pump pulse energy ($\lambda_p = 1941$ nm) at a pulse repetition rate of 0.5 kHz (*1*) and of the total average output power on the average pump power at a pulse repetition rate of 1 kHz (*2*).

Using the above photodetectors, we recorded parametric oscillation pulses in the mid-IR range and the pump radiation at the input or output of the nonlinear element. At the highest oscillation power, its pulse duration was comparable with the duration of the Tm^{3+}:YAP laser radiation pulse at the input of the crystal (Fig. 7a). The parametric oscillation spectrum included a broad line (FWHM: from ~3820 to ~3970 nm) with an inhomogeneous structure that changed from pulse to pulse (Fig. 7b). The oscillation took place near the 'degeneracy point' (at a wavelength of 3882 nm). The recorded generation beam corresponded to one transverse mode of the OPO cavity, a Gaussian beam with small distortions: the beam quality parameter determined by the 'knife technique' was $M_x \leqslant 3$, $M_y \leqslant 2–2.5$ (see the inset in Fig. 7b). At the highest output power, a weak red glow was also observed in the conversion region of the nonlinear element.

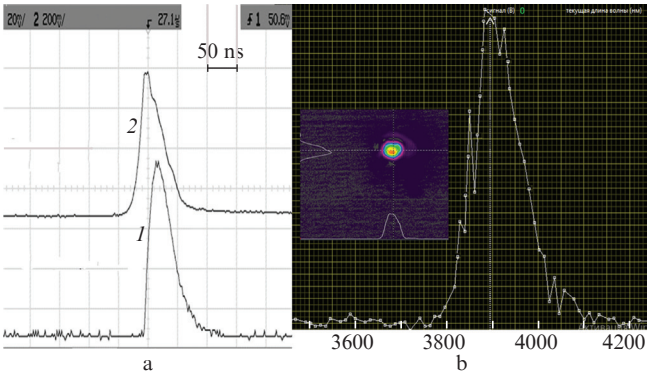

Figure 7. (Colour online) (a) Oscillograms of the parametric oscillation pulse (*1*) (after the filter) and the pump pulse (*2*) passed through the nonlinear crystal, as well as (b) the oscillation spectrum (in nm). The average output power is ~0.95 W at a pulse repetition rate of 1 kHz; the arrow in Fig. 7b shows the degeneracy wavelength of the parametric oscillation. The inset shows the output beam after the filter recorded by the Pyrocam IV camera.

4. Second harmonic generation

Preliminary estimates showed the possibility of frequency doubling (second harmonic generation) of Tm^{3+}:YAP laser radiation in the same PPMg:LN nonlinear element, though with a different period of the domain structure. Therefore, in the next experiment, the mirrors forming the OPO cavity were removed and the filter of the transmitted beam behind the nonlinear element was replaced. The new filter transmitted the radiation in the range 940–1000 nm (we used a dielectric mirror on a KU quartz substrate, which reflected radiation at a wavelength of 1941 nm with a coefficient $R > 99\%$ and transmitted radiation in the range 940–1000 nm with a coefficient $T \sim 96\%$). The radiation passing through the filter was directed to a spectrum analyser based on a SOLAR monochromator and a photodetector based on an FP 150 module (OJSC Polyus Research Institute). To focus the Tm^{3+}:YAP laser beam into a PPMg:LN crystal, a lens with $f = 70$ mm was used; the effective focal length, considering the beam divergence, was ~105 mm, the pump beam diameter in the nonlinear element was 190–200 μm, and the estimated Rayleigh length of the focal waist was 14.4–16 mm. The lens position relative to the PPMg:LN crystal was adjusted to maximise the nonlinear optical conversion efficiency.

During preliminary tuning of the SHG, the nonlinear element (as in the OPO experiment) moved in the transverse direction along the Y axis. At each position of the crystal, the temperature was varied in the range of 293–433 K. The tuning goal was the achievement of the highest radiation power at a wavelength of ~970.5 nm at the output of the monochromator. Preliminary tuning showed the presence of the desired second-harmonic emission when the beam passed through the region of the PPMg:LN element, opposite to that used in the OPO experiment. The grating period was estimated to be 28.5–28.7 μm, which corresponded to the optimal period of 28.6 μm at a temperature of ~410 K, according to SNLO. After preliminary finding of the position of the PPMg:LN element, its position and temperature were further adjusted to maximise the SHG power.

The second-harmonic pulses recorded by the photodetector were slightly shorter than the pumping pulses (Fig. 8a). The SHG spectrum contained a line at ~970.5 nm (Fig. 8b).

As a result of experiment optimisation, the energy of second-harmonic pulses amounted to 0.91 mJ at a pumping pulse energy of 2.7 mJ and a pulse repetition rate of 0.5 kHz (Fig. 9). The pulse energy conversion efficiency was as high as ~34%. The second harmonic beam recorded by the Pyrocam IV camera after passing through the filter had a close-to-Gaussian shape: the beam quality parameter $M_x \leqslant 4$, $M_y \leqslant 3$ (Fig. 9).

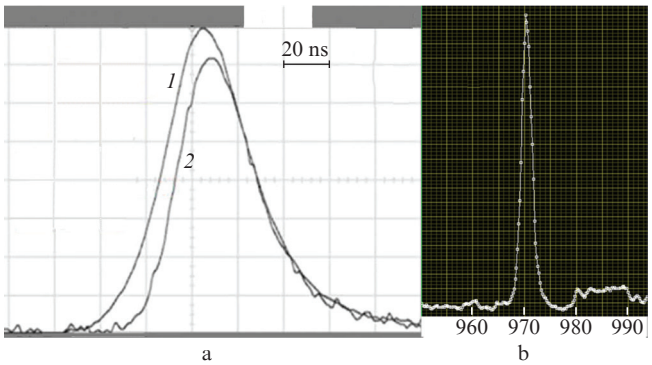

Figure 8. (a) Oscillograms of the pump pulses at $\lambda_p = 1941$ nm (*1*) and the second harmonic at $\lambda = 970.5$ nm (*2*) and (b) the SHG spectrum (in nm).

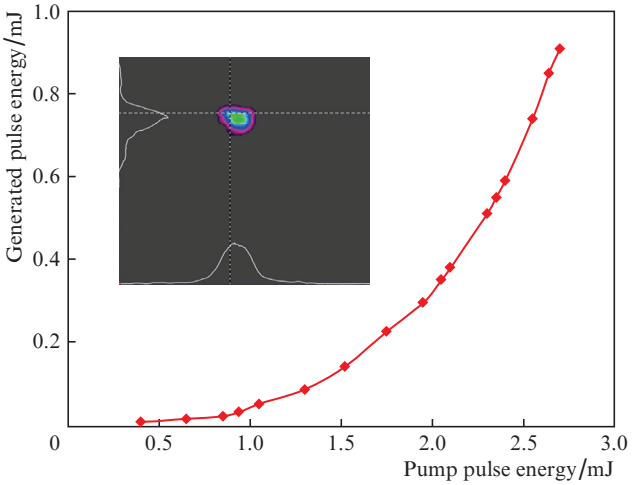

Figure 9. (Colour online) Energy of second-harmonic pulses as a function of the pump pulse energy at a pulse repetition rate of 0.5 kHz. The inset shows the shape of the second harmonic beam after the filter.

It should be noted that the optimal setting was accompanied, along with SHG, by visible radiation (glow) of red, blue-green, and white colours observed at the crystal output, which can be attributed to the generation of the sum frequency (pump + second harmonic) and the second SHG stage: generation of the 4th harmonic and the nonlinear conversion to higher-order harmonics. The presence of a stepwise conversion to higher harmonics can explain the limitation of the increase in the output power of the second harmonic.

5. Discussion of results

Parametric oscillation and SHG were implemented for the same pumping wavelength, $\lambda_p = 1941$ nm, and in one element, PPMg:LN, but for different periods of spontaneous domain polarisation in it. However, in previous experiments with the same PPMg:LN element, but with pumping at a wavelength of 1967 nm, the effects of parametric oscillation and SHG competed markedly [4]. The study of the temperature dependence of the optimal period of the PPMg:LN element using the SNLO program for degenerate parametric generation and SHG showed that at $\lambda_p = 1941$ nm these nonlinear optical effects are realised for different periods, while the wavelength $\lambda_p = 1967$ nm necessitates closer or identical periods (Fig. 10).

The effective nonlinearity coefficients d_{eff} for SHG and parametric oscillation under pumping at $\lambda_p = 1941$ and 1967 nm are approximately the same: ~14.9 and ~13.6 pm V^{-1}, respectively [49]. The linear absorption coefficients in a PPMg:LN crystal at parametric oscillation wavelengths in the range of 3880–3930 nm are also little different [14, 15]. Therefore, the stronger competition between parametric oscillation and SHG under pumping at a wavelength of 1967 nm than under pumping at 1941 nm can be explained by precisely the closeness of the optimal period PPMg:LN for these two effects at longer wavelength pumping.

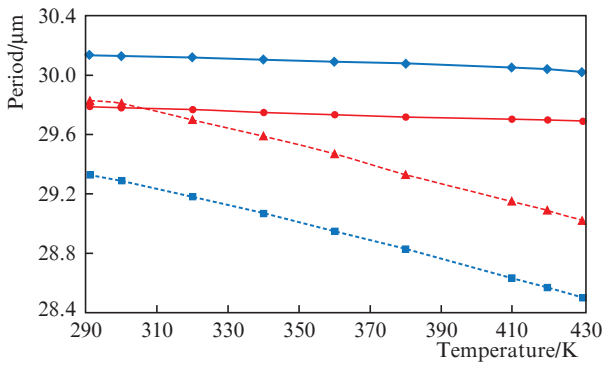

Figure 10. Temperature dependences of the optimal period of a PPMg:LN element with a regular domain structure for parametric generation in the degenerate regime (solid lines) and for SHG (dashed lines) at pump wavelengths of 1941 (blue lines) and 1967 nm (red lines).

A further increase in the output power of OPO and SHG in a PPMg:LN crystal pumped at λ_p = 1941 nm is possible with an increase in the power of laser pulses, for example, by shortening them. However, an increase in the power and energy density of laser pulses is limited by the optical damage of the elements of both the laser itself and the nonlinear optical crystal (especially when generating visible light in PPMg:LN [4]). Improvement of the optical quality of the PPMg:LN crystal and the use of a structure with a fixed period should also make it possible to increase the efficiency of the nonlinear optical conversions.

The use of pump radiation in the wavelength range 1985–1992 nm may entail a limitation on the power and energy of the OPO due to an increase in the absorption of laser beams in the PPMg:LN crystal at wavelengths longer than 4 μm [14, 15]. However, shortening the laser wavelength of the Tm^{3+}:YAP laser (to 1890–1897 nm) can lower the breakdown threshold of the laser elements and lead to thermal distortions of the pumping beam due to an increase in the absorption by water vapor in this spectral range [50].

6. Conclusions

Summarising the results, the repetitively pulsed output of a Tm^{3+}:YAP laser at 1941 nm served as an effective pump for OPO based on PPMg:LN crystals, which made it possible to obtain operation in the quasi-degenerate regime in the mid-IR wavelength range of 3820–3970 nm. In the same crystal, but with a different period of the domain structure, it was possible to implement SHG of laser radiation at 1941 nm and obtain a high-power beam of coherent radiation at 970.5 nm.

Acknowledgements. This research was supported by the Ministry of Science and Higher Education of the Russian Federation (within the framework of the State Assignment for the IAP RAS, Project No. 0030-2021-0012, and the State Assignment for Novosibirsk State University, Project FSUS 2020-0036) and the Russian Science Foundation (Project No. 19-12-00085) with the use of the equipment of the Ural Centre for Collective Use 'Modern Nanotechnologies' of Ural Federal University (Registration No. 2968).

References

1. Scholle K., Lamrini S., Koopmann P., Fuhrberg P. *Frontiers in Guided Wave Optics and Optoelectronics* (Croatia: InTech, 2010) pp 471–500.
2. Vodopyanov K.L. *Laser-based Mid-infrared Sources and Applications* (Wiley, USA: 2020) p. 287.
3. Xu L., Liang S., Fu Q., Shepherd D.P., Richardson D.J., Alam S. *Appl. Phys. B*, **124** (59), 44 (2018).
4. Antipov O., Kolker D., Kal'yanov D., Larin S., Shur V., Akhmathanov A. *J. Opt. Soc. Am. B*, **35** (7), 1674 (2018).
5. Budni P.A., Pomeranz L.A., Lemons M.L., Miller C.A., Mosto J.R., Chicklis E.P. *J. Opt. Soc. Am. B*, **17**, 723 (2000).
6. Zakharov N.G., Antipov O.L., Sharkov V.V., Savikin A.P. *Quantum Electron.*, **40** (2), 98 (2010) [*Kvantovaya Elektron.*, **40** (2), 98 (2010)].
7. Antipov O.L., Kositsyn R.I., Eranov I.D. *Laser Phys. Lett.*, **14** (1), 015002 (2017).
8. Zhao Ben-Rui, Yao Bao-Quan, Qian Chuan-Peng, Liu Gao-You, Chen Yi, Wang Rui-Xue, Dai Tong-Yu, Duan Xiao-Ming. *Opt. Lett.*, **43** (24), 5989 (2018).
9. Haakestad M.W., Fonnum H., Lippert E. *Opt. Express*, **22** (7), 8556 (2014).
10. Liu G., Mi S., Yang K., Wei D., Li J., Yao B., Yang C., Dai T., Duan X., Tian L., Ju Y. *Opt. Lett.*, **46** (1), 82 (2021).
11. Schunemann P.G., Zawilski K.T., Pomeranz L.A., Creeden D.J., Budni P.A. *J. Opt. Soc. Am. B*, **33** (11), D36 (2016).
12. Zawilski K.T., Setzler S.D., Schunemann P.G., Pollak T.M. *J. Opt. Soc. Am. B*, **23**, 2310 (2006).
13. Yudin N.N., Antipov O.L., Gribenyukov A.I., Eranov I.D., Podzyvalov S.N., Zinov'ev M.M., Voronin L.A., Zhuravleva E.V., Zykova M.P. *Quantum Electron.*, **51** (4), 306 (2021) [*Kvantovaya Elektron.*, **51** (4), 306 (2021)].
14. Myers L.E., Eckardt R.C., Fejer M.M., Byer R.L., Bosenberg W.R., Pierce J.W. *J. Opt. Soc. Am. B*, **12**, 2102 (1995).
15. Hum D.S., Fejer M.M. *Compt. Res. Phys.*, **8**, 180 (2007).
16. Dmitriev V.G., Tarasov L.V. *Prikladnaya nelineinaya optika* (*Applied Nonlinear Optics*) (Moscow: Fizmatlit, 2004) Ch. VII, p. 366.
17. Petrov V. *Opt. Mater.*, **34** (3), 536 (2012).
18. Shen Y., Alam S., Chen K.K., Lin D., Cai S., Wu B., Jiang P., Malinowski A., Richardson D.J. *IEEE J. Sel. Top. Quantum Electron.*, **15** (2), 385 (2009).
19. Adler F., Cossel K.C., Thorpe M.J., Hartl I., Fermann M.E., Ye J. *Opt. Lett.*, **34** (9), 1330 (2009).
20. Wu B., Kong J., Shen Y. *Opt. Lett.*, **35** (8), 1118 (2010).
21. Chaitanya Kumar S., Das R., Samanta G.K., Ebrahim-Zadeh M. *Appl. Phys. B*, **102** (1), 31 (2011).
22. Lin D., Alam S., Shen Y., Chen T., Wu B., Richardson D.J. *Opt. Express*, **20** (14), 15008 (2012).
23. He Y., Ji Y., Wan H., Yu D., Zhang K., Pan Q., Sun J., Chen Y., Chen F. *Opt. Laser Technol.*, **146**, 107545 (2022).
24. Larionov I.A., Gulyashko A.S., Alekseev D.A., Tyrtyshnyy V.A., in *Techn. Digest Intern. Conf. Laser Opt.*, 2020 (on-line), TuSYA-13.
25. Honea E., Savage-Leuchs M., Bowers M.S., Yimaz T., Mead R. *Proc. SPIE*, **8601**, 860111 (2013).
26. Creeden D., Blanchard J., Pretorius H., Limongelli J., Setzler S. *Proc. SPIE*, **9728**, 972829 (2016).
27. Xu L., Liang S., Fu Q., Shepherd D.P., Richardson D.J., Alam S. *Appl. Phys. B*, **124** (59) (2018).
28. Hansson G., Smith D.D. *Appl. Opt.*, **37**, 5743 (1998).
29. Hansson G., Smith D.D. *Opt. Lett.*, **25**, 1783 (2000).
30. Bao Z.X., Yao B.Q., Ju Y.L., Wong Y.Z. *Chines Phys. Lett.*, **24**, 1953 (2007).
31. Kolker D.B., Antipov O.L., Larin S.V., Isaenko L.I., Vedenyapin V.N., Akhmatkhanov A.R., Shur V.Ya. *Opt. Atmos. Okeana*, **32** (8), 669 (2019).
32. Cole B., Goldberg L., Hays A.D. *Opt. Lett.*, **43** (2), 170 (2018).
33. Cole B., Goldberg L., Chinn S., Pomeranz L.A., Zawilski K.T., Schunemann P.G., McCarthy J. *Opt. Lett.*, **43** (5), 1099 (2021).

34. Mi S., Li J., Wei D., Yang K., Yang C., Yao B., Duan X., Dai T. *Opt. Laser Technol.*, **138**, 106847 (2021).
35. Kalachev Yu.L., Mihailov V.A., Podreshetnikov V.V., Shcherbakov I.A. *Opt. Commun.*, **284** (13), 3357 (2011).
36. Antipov O., Novikov A., Larin S., Obronov I. *Opt. Lett.*, **41**, 2298 (2016).
37. Antipov O.L., Getmanovskiy Yu.A., Dobrynin A.A., Huang H.T., Shen D.Y., Wang J., Balabanov S.S. *Appl. Phys. B*, **127** (77) (2021).
38. Larin S., Antipov O., Sypin V., Vershinin O. *Opt. Lett.*, **39** (11), 3216 (2014).
39. Diehl R., Brandt G. *Mater. Res. Bull.*, **10** (2), 85 (1975).
40. Antipov O.L., Getmanovskiy Yu.A., Dobrynin A.A., Shestakova I.A., Shestakov A.V., Balabanov S.S., Larin S.V. in *Techn. Digest CLEO/Europe 2021* (on-line), CA-P.17.
41. Antipov O.L., Getmanovskiy Yu.A., Balabanov S.S., Larin S.V., Sharkov V.V. *Laser Phys. Lett.*, **18**, 055001 (2021).
42. www.rezonator.orion-project.org.
43. Aggarwal R.L., Ripin D.J., Ochoa J.R., Fan T.Y. *J. Appl. Phys.*, **98** (10), 103514 (2005).
44. ISO 11146-1:2005, *Lasers and laser-related equipment -Test methods for laser beam widths, divergence angles and beam propagation ratios*.
45. Powers P.E., Kulp Th.J., Bisson S.E. *Opt. Lett.*, **23** (3), 159 (1998).
46. Shur V.Ya., Akhmatkhanov A.R., Baturin I.S. *Appl. Phys. Rev.*, **2**, 40604 (2015).
47. Ren T., Wu Ch., Yu Y., Dai T., Chen F., Pan Q. *Appl. Sci.*, **11**, 11451 (2021).
48. Paul O., Quosig A., Bauer T., Nittmann M., Bartschke J., Anstett G.,L, Huillier J.A. *Appl. Phys. B*, **86** (1), 111 (2006).
49. https://as-photonics.com/products/snlo/.
50. https://hitran.iao.ru/.